7. Francis Bacon is often cited as having pointed out the unusually good fit of the continents, in a passage in *The New Organon* (1620), but a close examination of the passage suggests that Bacon was probably referring only to the similarity of shapes of two western coasts, rather than to the fit of an east coast with a west coast.
8. For a comprehensive history of the theory of continental drift, see U. B. Marvin, *Continental Drift* (Smithsonian Institution Press, Washington, DC, 1973). For a discussion of Wegener, see N. Oreskes, *Hist. Stud. Phys. Biol. Sci.* **18**, 311 (1988).
9. J. Ray, *The Wisdom of God Manifested in the Works of the Creation* (1704) (Samuel Smith, London, 1704).
10. J. J. Rousseau, *Profession of Faith of a Savoyard Vicar* (1765), trans. in *Harvard Classics*, C. W. Eliot, Ed. (P. F. Collier and Son, New York, 1910), vol. 34.
11. C. Darwin, *The Origin of Species* (1859) (Collier Books, New York, 1962).
12. Galileo, *De Motu* (1592), trans. in *Galileo on Motion and on Mechanics* by I. E. Drabkin and S. Drake (Univ. of Wisconsin Press, Madison, 1960).
13. I. Newton, *System of the World*, F. Cajori, Ed. (Univ. of California Press, Berkeley, 1934), sect. 19.
14. R. V. Eotvos, *Math. Naturw. Ber. Ungarn* **8**, 65 (1889).
15. A. Einstein, *Ann. Phys.* **35**, 898 (1911), trans. in *The Principle of Relativity* by H. A. Lorentz, A. Einstein, H. Minkowski, and H. Weyl (Dover, New York, 1952).
16. Aristotle, *Posterior Analytics*, 1.13. In the Middle Ages the fact-in-itself was called a *quia* and the reasoned fact was called a *propter quid.*
17. B. Barber, *Science* **134**, 596 (1961).
18. L. Festinger, *A Theory of Cognitive Dissonance* (Stanford Univ. Press, Stanford, CA, 1957), p. 3.
19. For helpful discussion and comments we thank R. Brawer, S. Brush, P. Galison, S. J. Gould, G. Holton, H. Margolis, U. Marvin, A. Pickering, H. Ritvo, and F. Sulloway.

Deformational Mass Transport and Invasive Processes in Soil Evolution

GEORGE H BRIMHALL,* OLIVER A. CHADWICK, CHRIS J. LEWIS, WILLIAM COMPSTON, IAN S. WILLIAMS, KATHY J. DANTI, WILLIAM E. DIETRICH, MARY E. POWER, DAVID HENDRICKS, JAMES BRATT

Soils are differentiated vertically by coupled chemical, mechanical, and biological transport processes. Soil properties vary with depth, depending on the subsurface stresses, the extent of mixing, and the balance between mass removal in solution or suspension and mass accumulation near the surface. Channels left by decayed roots and burrowing animals allow organic and inorganic detritus and precipitates to move through the soil from above. Accumulation occurs at depths where small pores restrict further passage. Consecutive phases of translocation and root growth stir the soil; these processes constitute an invasive dilatational process that leads to positive cumulative strains. In contrast, below the depth of root penetration and mass additions, mineral dissolution by descending organic acids leads to internal collapse under overburden load. This softened and condensed precursor horizon is transformed into soil by biological activity, which stirs and expands the evolving residuum by invasion by roots and macropore networks that allows mixing of materials from above.

SOILS AND WEATHERED BEDROCK FORM THE BASAL PORTION of open biogeochemical ecosystems at the interface of the atmosphere, biosphere, hydrosphere, and subaerial lithosphere (*1*). In an effort to define the role of soils in global change, researchers have considered soils to act as the earth's geomembrane (*2*), with some behavior analogous to that of biomembranes of living organisms (*3*). The term geomembrane implies that interfacial transport processes are regulated and raises the central questions of how transport occurs in soils, how organisms in the soil community (*4, 5*) influence transport processes, and how soils decompose rocks. In this article we examine the theory that vertical evolution of soil formed in place (not on steep hillslopes) is a consequence of spontaneous dynamic interaction of the biota and waste-product organic acids with rock minerals derived both from the underlying rock and from eolian sources. This interaction is governed by nonequilibrium thermodynamics, mechanics, mass transport, and ground-water flow in the rock-soil-plant system. We quantify and interpret modes and rates of interaction among organisms, transported materials, and the minerals that compose weathered rocks in these invasive interfacial systems.

Mass fluxes between different portions of chemical weathering and soil forming systems are particularly useful monitors of near surface transport processes. They serve as natural chemical tracers indicative of the extent of erosion (*6*), source, pathway, and reservoir regions (*7*), and can be related directly to observed soil features (*8–11*). Because mass fluxes in soils are computed from mass conservation volume-density-composition relations, it is imperative to evaluate the effects of volume change. Deformation and buckling of concrete sidewalks by root growth provide vivid and familiar evidence that volume changes attributable to common stresses do occur near the surface in soils.

Mass balance modeling techniques yielding chemical gains and losses that attend chemical weathering and soil formation have evolved considerably in their treatment of volume change. Initially, and until recently, isovolumetric reactions were assumed (*6, 12–14*)

G. H Brimhall, C. J. Lewis, K. J. Danti, and W. E. Dietrich are with the Department of Geology and Geophysics, University of California, Berkeley, CA 94720. O. A. Chadwick is with the Jet Propulsion Laboratory, California Institute of Technology, Pasadena, CA 91109. W. Compston and I. S. Williams are with the Research School of Earth Sciences, Australian National University, Canberra ACT 2601, Australia. M. E. Power is in the Department of Integrative Biology, University of California, Berkeley, CA 94720. D. Hendricks is in the Department of Soil and Water Science, University of Arizona, Tucson, AZ 85721. J. Bratt is with BHP-Utah International Metals, 550 California Street, San Francisco, CA 94104.

*To whom correspondence should be addressed.

or ratios of presumed immobile elements were used to normalize chemical concentrations (*15*). In contrast, our purpose here is to apply recent formal mass balance models (*7–11*) to quantify and better understand the various roles of deformation and to define their interplay with mass transport processes and biological activity.

Natural soil deformation under transient or constant loads has been quantified in many applications, for example, landslides, soil creep, and tillage-induced compaction (*16–19*), but studies coordinating deformation with other surface processes, such as chemical or thermal effects, are less common. Two examples of abiotically induced thermomechanical strain are (i) cracking in vertisols attributed to alternating shrink-swell behavior of expandable clays that change volume in response to hydration-desiccation cycles (*20, 21*) and (ii) mass displacement in frozen soils by frost wedging in an active layer above permafrost (*22*).

Clarifying the role and interrelation between deformation and mass transport during soil evolution and rock weathering is critical to understanding surface processes and their response to global change. For example, aridification, resulting both in remobilization of copper (*7, 23*) and reduction in erosion rate, has led to surficial enrichment and preservation of certain ore deposits (*24*). Eolian dust deposition has been shown to be an important feature of the genesis of lateritic bauxite deposits (*9*), and gold in some deposits has been concentrated mechanically in the subsurface during lateritic weathering (*10*).

Strain and Mass Transport Analysis

Recent development of a physiochemical strain gauge (*8–10*) based on mass balance has allowed researchers to determine the amount and sense of deformation in soils and hence to use the accumulated strain to calculate chemical gains and losses. The overall conservation of mass of any chemical element, j, can be expressed in terms of the product of volume (V in cubic centimeters), dry bulk density (ρ in grams per cubic centimeter), and chemical composition (C in weight percent) plus the accumulated mass fluxes ($m_{j,\text{flux}}$) into or out of the system, where "p" refers to the parent material and "w" refers to its weathered product:

$$\frac{V_p \rho_p C_{j,p}}{100} + m_{j,\text{flux}} = \frac{V_w \rho_w C_{j,w}}{100} \quad (1)$$

Fluxes are positive if they enter the system and negative if they leave the system. Rather than rely on an assumed isovolume frame of reference, we identify insoluble host minerals containing immobile elements, i, and solve Eq. 1 for strain, $\varepsilon_{i,w}$, defined as $(V_w - V_p)/V_p$, which reduces to Eq. 2 for an immobile element for which $m_{i,\text{flux}}$ is equal to zero:

$$\varepsilon_{i,w} = \frac{\rho_p C_{i,p}}{\rho_w C_{i,w}} - 1 \quad (2)$$

Positive strains are dilations and negative strains represent collapse. Collapse is indicated by Eq. 2 when the increase in concentration of an immobile element ($C_{i,w}$) caused by loss of mobile constituents is not exactly compensated by an inversely proportional decrease in bulk density (ρ_w) due to increasing porosity such that the product of $C_{i,w}$ and ρ_w remains constant. Clearly, the definition of strain given in Eq. 2 treats only bulk volume change, ignoring distortion and offering no information about the direction of volume change, and relies on sample size being sufficiently large to constitute a representative sample of a homogeneous media. The representative elementary volume (REV) used in our analysis is a sample volume of 132 cm^3 (*10*).

Once the bulk strain is computed from Eq. 2, absolute chemical mass gains and losses per unit volume of parent material, $\delta_{j,w}$, are calculated with Eq. 3, or mass fractions, $\tau_{j,w}$, relative to the mass of element, j, in the parent material are calculated with Eq. 4.

$$\delta_{j,w} = \frac{m_{j,\text{flux}}}{V_p} = \frac{\rho_w C_{j,w}(\varepsilon_{i,w} + 1) - \rho_p C_{j,p}}{100} \quad (3)$$

$$\tau_{j,w} = 100 \frac{m_{j,\text{flux}}}{V_p C_{j,p} \rho_p} = \frac{\rho_w C_{j,w}}{\rho_p C_{j,p}} (\varepsilon_{i,w} + 1) - 1 \quad (4)$$

Development of Soils

We have evaluated the biogeochemical mechanics and progressive development of soils over two distinct time scales by analyzing (i) the mechanisms of in situ development as a function of time when communities colonize freshly exposed geological substrates and evolve for periods up to 240,000 years and (ii) the long-term record of soil evolution in ancient cratonal soils developed over millions of years.

Soils originate when bacteria, fungi, algae, lichens, and vascular plants colonize freshly exposed geological substrates. One can study soil development by using chronosequence concepts in which the effects of dominant nonchronological controls on soil evolution (climate and climate change, organisms, topography, and parent material) are minimized by careful field-site selection (*4, 5*). As an example of strain analysis in reference to mass transport applied to soil development in a humid temperate environment, we sampled soil profiles that form a time history of soil evolution in beach sand (*25–29*). Seven soil profiles were sampled on six gently sloping (1° to 4°) marine terraces formed over the past 240,000 years near the mouth of the Mattole River, northern California. Many aspects of morphological, mineralogical, and chemical development of these profiles have been quantified relative to sand on the present beach that represents the parent material for each profile (*26, 27*). Here, we quantify soil deformation in response to biogeochemical mass fluxes.

Plots of $\varepsilon_{Zr,w}$ versus depth (Fig. 1A) for each profile indicate that the soils evolved from dilation (positive strain) to collapse (negative strain) as they became established and aged. In the younger terraces, the greatest dilation occurs near the surface. In the younger profiles [3.9 to 29 ka (thousand years ago)], dilation decreases with depth to a point where near zero strain is reached; the older soils (40 to 240 ka) are dilated near the surface but collapsed within the first meter below the surface. These observations suggest that as soils age, the amount of dilation near the surface decreases, the extent of collapse increases, and the point of crossover between dilation and collapse ascends toward the surface.

A plot of average strain for each profile, integrated over the sampling depth, versus terrace age (Fig. 1B) indicates that initially the soils dilated rapidly, but then they followed a linear collapse through time. In soils that formed over the last 40,000 years, collapse has just begun, whereas in soils that began forming 240 ka, nearly 40% of their volume has been lost. These relations imply that cumulic processes dominated during the early stages of these soils but mineral dissolution and leaching processes dominated as they matured. Initially, there were dramatic increases in Si (Fig. 1C) by eolian additions of quartz-rich sand (a strand of barbed wire is buried under 20 cm of eolian sand on the 3.9-ka terrace). At the same time, organic carbon (OC) (Fig. 1D) became incorporated into the soil as vegetation was established. The profile shows that incorporation of eolian sand and OC, associated with strong dilation (>30%) of the soil, diluted the concentration of immobile trace elements such as Zr ($C_{Zr,w}$) and lowered ρ_w (Eq. 2). Silicon and OC are important controlling variables for soil deformation because they

are the most abundant component in the soils (with the exception of oxygen) and show the greatest percent change relative to parent material concentrations, respectively, (*11*). In contrast, Fe and Al have undergone only minor mass changes.

The cumulic phase of soil development in these soils was intense but of short duration because eolian flux and OC accumulation decreased rapidly after the formation of each terrace. The drop in sea level after interglacial or interstadial eustatic sea-level highstands and the rapid coastal uplift (~4 mm per year) removed newly formed terraces from the active eolian zone. The rate of OC accumulation slowed rapidly once dynamic equilibrium between OC input and breakdown was reached (*5*). The amount of eolian additions varies among nearby profiles (thus, the calculated dilatational strain varies); for this reason the soil on the youngest terrace (3.9 ka) may not be representative, and we thus developed best-fit predictive curves both with and without these data (Fig. 1, B and C).

Compared with cumulic processes, mineral weathering and leaching are less spatially variable but slower to leave a quantifiable impact. However, in the 29-ka soil, the concentration of Si is much less than that in the younger soil and is similar to that of the beach sand; the OC concentration has only increased by 50% over the value in the soil on the 3.9-ka terrace. Average integrated dilation in the 29-ka soil is less than 20%. Comparison of the soils on the 29- to 240-ka terraces shows that Si mass loss and average collapse increase with age. If we include data from the 3.9-ka terrace, average collapse is still linear (Fig. 1B), but Si loss is nonlinear (Fig. 1C), as is OC gain (Fig. 1D). Elemental mass balance and mineralogical studies indicate that soil collapse is due to leaching of Si and cations released by hydrolysis of plagioclase and other weatherable minerals, which increases the concentration of immobile Zr in the soils occurring as unweathered zircon (Fig. 1, E and F) (*11*). Collapse is partly offset by additions of OC and eolian minerals, but the higher transition point between dilation and collapse in the older soils indicates that desilication is the most important long-term factor in soil deformation. In young soils, accumulation of OC and eolian input predominate over Si loss. Hence, dilation occurs.

Morphostratigraphic studies have shown that the present beach sand is representative of the parent material of each soil profile (*26, 27*). Thus, we can document colonization of geologic substrate and chemical evolution of the soil profile by comparing soil composition with that of the sand. Our model for soil evolution is that vegetation growth traps eolian sand in the near-beach environment and incorporates organic matter into the growing soil. Low molecular weight organic acids released in root exudates and microbial breakdown of organic matter fuel long-term hydrolytic weathering of silicate minerals. Early in the development of a soil, desilication is a by-product of nutrient release. Long-term evolution of the soil may lead to exhaustion of nutrient-supplying minerals, as in the case of the Blacklock soil in the Pygmy Forest along the Mendocino coast of California (*5*). In most cases, however, long-term soil evolution is subject to changes in external stimuli, such as increased erosion or modification in the rate of eolian dust deposition. Mass balance and micromorphologic interpretations of older soils allow detailed evaluation of more complex soil function.

Long-Term Evolution of Soils

Long-term natural pedogenic processes, including deformation occurring over time spans of millennia or millions of years and depths exceeding tens of meters, can be understood by study of ancient soil profiles formed on tectonically inactive cratons. Here, the antiquity of soils and slow erosion rates allow study of extreme states of soil development, including (i) mass exchange between well-developed soil reactor compartments, (ii) the upward evolutionary sequence (*30–32*), and (iii) the prolonged effects of regional dust deposition of a chemically mature eclectic mixture of foreign detritus on soil mechanics (*9, 10*). The soil profiles we have studied are lateritic bauxite deposits in Western Australia. These soils, widespread on cratons, are thick and chemically mature soils of global geological, economic, and agricultural importance that have been studied intensively by numerous workers (*9*).

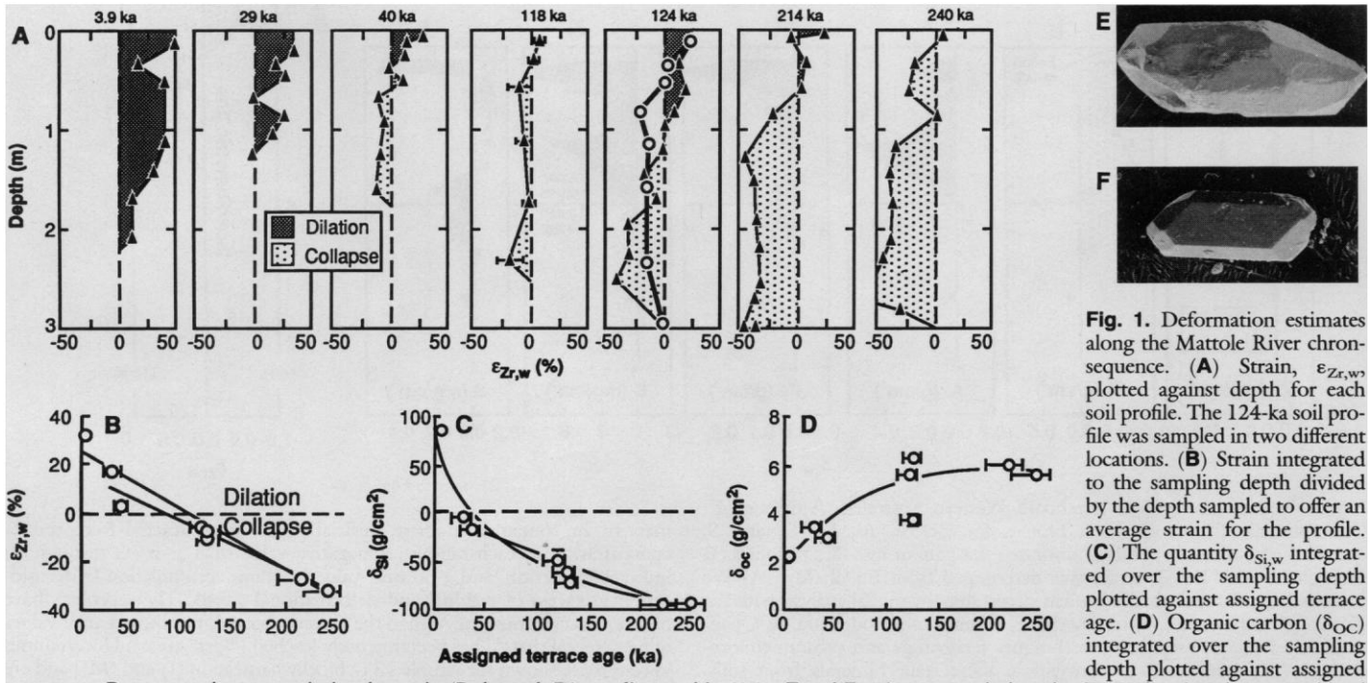

Fig. 1. Deformation estimates along the Mattole River chronsequence. (**A**) Strain, $\varepsilon_{Zr,w}$, plotted against depth for each soil profile. The 124-ka soil profile was sampled in two different locations. (**B**) Strain integrated to the sampling depth divided by the depth sampled to offer an average strain for the profile. (**C**) The quantity $\delta_{Si,w}$ integrated over the sampling depth plotted against assigned terrace age. (**D**) Organic carbon (δ_{OC}) integrated over the sampling depth plotted against assigned terrace age. Representative uncertainties shown in (B through D) are discussed in (*27*). (**E** and **F**) Zircon morphology by SEM, showing the unweathered character of these strain index minerals from 1-m depth in the 3.9- and 240-ka soils, respectively. Zircons are 260 μm long in (E) and 190 μm long in (F).

The Jarrahdale bauxite deposits in the Darling Range of Western Australia near Perth (*9*) are developed on Archean granitic gneiss parent material. Using Eq. 3, we transformed conventional geochemical profiles for Zr, Si, Al, Fe, C, and S (Fig. 2, A to F) into chemical mass gains and losses (Fig. 2, G to L). These mass budgets are based on a strain profile (Fig. 2M) calculated from Eq. 2. Because a distinctive, abraded, heavy-mineral suite consisting of rounded zircon, rutile, and ilmenite (*9, 33*) is recognized as a contaminant in the upper meter of the profile, we corrected the Zr concentrations by subtracting the amount of Zr contributed by foreign zircon using a digitizing microscope for accurate modal counting of trace minerals in quantitative heavy-mineral concentrates (*34, 35*) (Fig. 2A).

In addition to contamination by the abraded detrital mineral suite, the upper parts of the bauxites have also accumulated Al, Fe, C, and S compounds (Fig. 2, I to L). Although the magnitude of Al, Fe, and C accumulation is significant, this net mass gain is more than offset by pervasive loss of Si (Fig. 2H), which has caused a reduction in bulk density on the order of almost 1 g/cm^3, as in the oldest of the Mattole River soils. The depth of C accumulation by biochemical cycling of organic components (Fig. 2K) is roughly coincident with the depth of modern root growth (Fig. 2G) and is also similar to the maximum depth of Al- and Fe-rich mineral infillings in biopores created by roots (Fig. 2, I and J). We conclude, therefore, that the soil column can be divided into two functional layers. Within a near surface bioturbated layer, continuous macropores focus the downward translocation of indigenous and foreign particles. Below this contaminated zone the much smaller microscopic pores preclude further translocation of detrital minerals from above. Hence, intense leaching of Si and Al species by hydrolysis of silicate minerals, largely feldspars, predominates chemical gains and losses.

Separating the upper and lower soil systems is what we term a translocation crossover (TCO) (*36*), where mass accumulation by invasive downward translocation ceases (for Fe and C) or, for certain elements (Al), even becomes negative where net mass loss occurs. Surprisingly, Al is leached (Fig. 2I) even though the Al concentration is higher than that in the parent material (Fig. 2C), an effect that could not have been recognized with the use of previous isovolumetric interpretive methods (*12, 13, 37*).

Direct evidence of the complex and heterogeneous strain indicat-

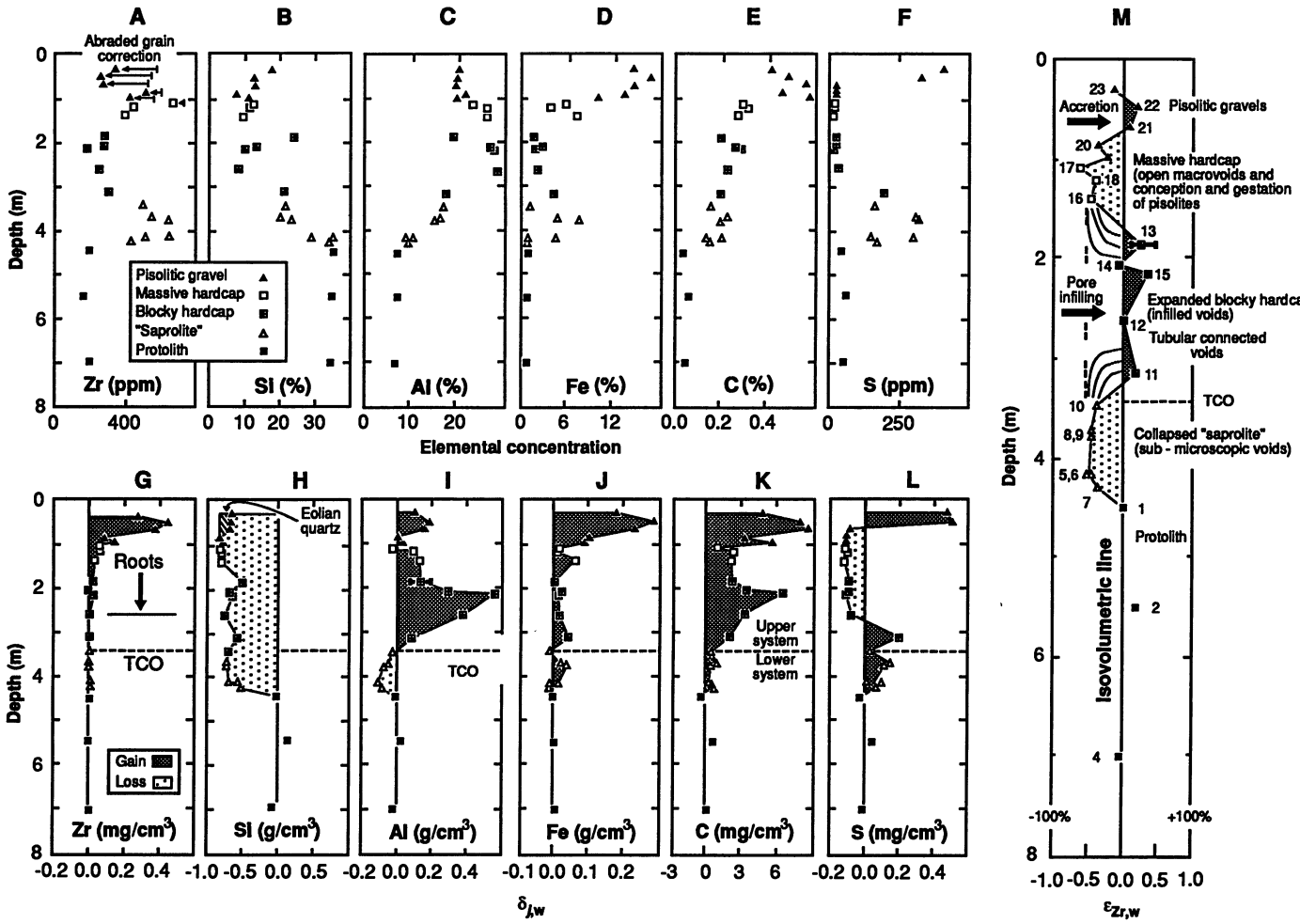

Fig. 2. Bauxite profile from Jarrahdale, Western Australia. (**A** through **F**) Conventional (C_j) geochemical profiles for Zr, Si, Al, Fe, C, and S, transformed into corresponding absolute mass gain or loss ($\delta_{j,w}$) profiles (**G** through **L**) with Eq. 3; strain was determined from Eq. 2 (**M**). (A) We corrected C_{Zr} data for abraded eolian zircon suite by modal analysis with the digitizing microscope (*34*) to determine volumes of rounded grains. Quantitative heavy liquid separation techniques (centrifuge and vacuum concentration) (*35*) were used to concentrate these trace minerals from soils. Conversion from a volumetric to a gravimetric basis with mineral densities gives the mass of abraded foreign zircon. Given the Zr content of zircon, the mass of Zr contained in these surficial phases is subtracted from the Zr concentration in each sample. A negative value of $\delta_{j,w}$ in (G through L) indicates depletion, and a positive value indicates accumulation by translocation in excess of residual and deformational effects. The saprolites have higher concentrations of Al than the parent material, but the negative values of $\delta_{Al,w}$ reveal that Al has been intensely leached ("loss" areas). Uncertainties in results are shown for sample 13 [a blocky hardcap in (I) and (M)] and are based on use of the maximum and minimum values of Zr concentration in the parent material.

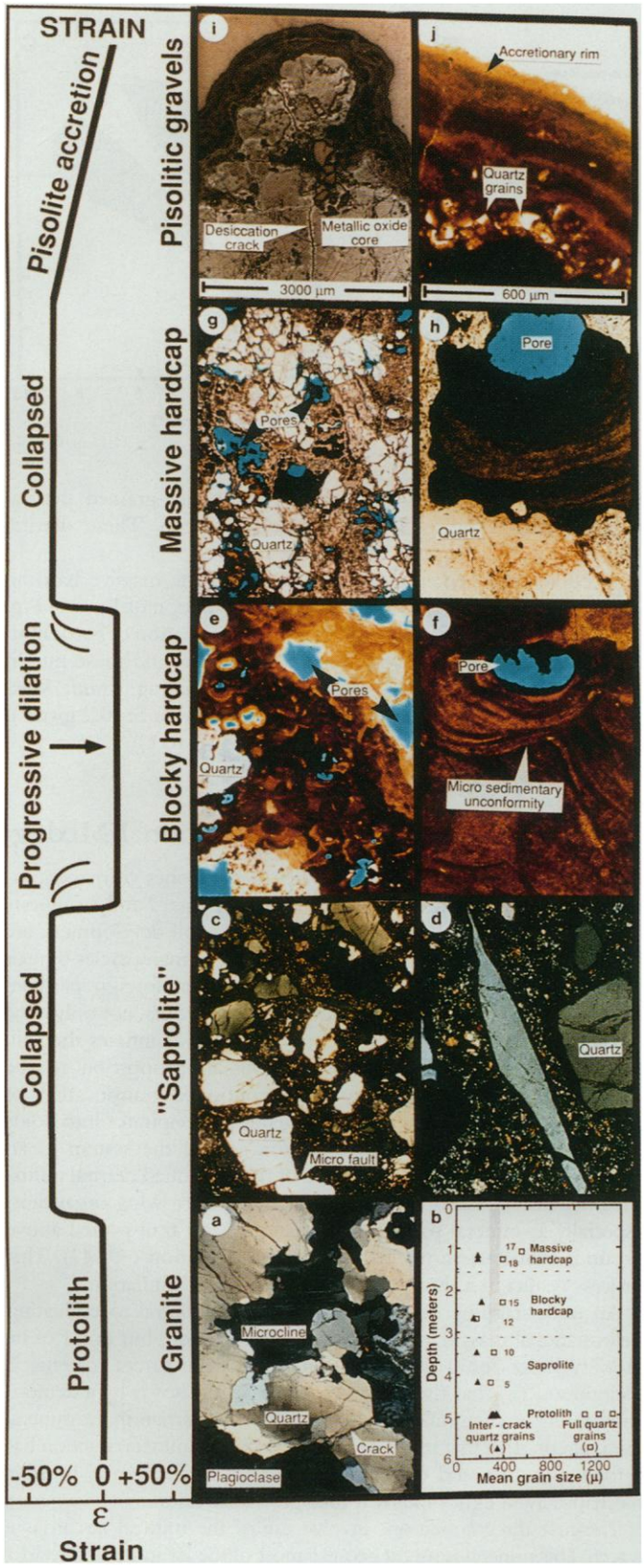

Fig. 3. Photomicrographic evolution of bauxite profile from (**a**) Archean gneissic granite parent material through (**c** and **d**) saprolite, (**g** and **h**) massive hardcap, and (**e** and **f**) blocky hardcap to (**i** and **j**) pisolitic gravel, shown at low magnification (left) and higher magnification (right). (**b**) Shows 1200-μm-diameter mosaic protolith quartz grains in relation to the 400-μm-diameter angular quartz fragments in (c) and (d). Quartz dissolution appears to have been negligible. Voids are blue-colored.

ed in Fig. 2M can be observed microscopically (Fig. 3) and related to mass flux budgets in a sequence of steps from which the biogeochemical mechanics of weathering emerge. At depth, saprolite occurring immediately above the granitic gneiss bedrock has not formed by an isovolumetric transformation but instead is highly collapsed, having shrunk to about one-half of its original volume. The fabric of the saprolite departs markedly from that of the gneiss (Fig. 3c). Loss of Si (Fig. 2H) by dissolution of feldspars (plagioclase and microcline) has controlled this collapse. In contrast, quartz has not dissolved appreciably but has simply broken into smaller (400 μm in diameter) fragments; the size of fragments reflects the spacing of microcracks in the mosaic quartz grains (1200 μm diameter) of the gneiss (Fig. 3b). Because the smaller quartz fragments remaining after dissolution of feldspar and dislocation of larger quartz grains are not in contact in the saprolite (Fig. 3, a and d), there is little resistance to dissolutional collapse and the saprolite becomes only matrix-supported, not grain-supported. Thus, breaking of the quartz grains into smaller angular pieces is a critical part of saprolite formation (Fig. 3d). Because of the intensity of chemical and physical modification of the saprolite and its position immediately below the TCO, we call it protosoil. This chemically primitive material represents the lowest soil compartment and is free of the invasive influence of surficial detritus introduced through tubular voids in the soil above. Thus, the TCO helps to eliminate a need for an arbitrary definition of the base of soil (*5*).

Above the protosoil, duricrust hardcap zones are characterized by tubular voids created by roots (Fig. 3, e through h); these voids contrast markedly with the submicroscopic pores of the protosoil. They are large, connected openings that control translocation and are partially infilled with oriented subhorizontal layers of aluminous and feruginous clay (Fig. 2, I and J) (*9*). The microlayering demonstrates that a cumulative soil-forming process (*38*) was operative, in which episodic additions of parent material occurred at the top of the soil. Comparing these micromorphological features with the strain curve shows that the massive hardcap (Fig. 3, g and h) remains in the collapsed state of its immediate progenitor "saprolite" protosoil, whereas the blocky hardcap expanded from −50% to over +20%, a net change of about +70%. Expansion has occurred as a result of many generations of root growth and microsedimentary infillings, as indicated by superimposed and crosscutting microsedimentary unconformities (Fig. 3f). Only the last few stages of textural reorganization survive as discernible sedimentary unconformities; evidence of the earlier stages is preserved only in the cryptic record of physical properties and chemical composition of the hardcap.

At the top of the profile a layer of pisolitic gravels develops. Accretionary spherical growth occurs by attachment of eolian and indigenous mineral grains to iron oxide cores (Fig. 3j). The gravel is a grain-supported aggregate with discrete pisolites touching tangentially. Because growth is accretionary, the amount of expansion increases upward toward the surficial source of quartz and ferruginous material. With accretion, pisolite centers move farther apart and contribute to dilation.

The interrelation between mass transport and deformation is evident from the strain-transport-time (STT) paths (Fig. 4) (*36*). Although there are no absolute age data on the individual depth zones in the bauxite, their development within the weathering profile has evidently occurred in general by a sequence of progressive replacement steps from a progenitor resembling that currently underlying each of them (*39*). The most recent material to form is at the base of the profile, and the most mature material is on top. Evidence that simultaneous advance of the interfaces has occurred and that these interfaces are functionally related to each other is evident in the character of the pathways (Fig. 4). Chemical gains and

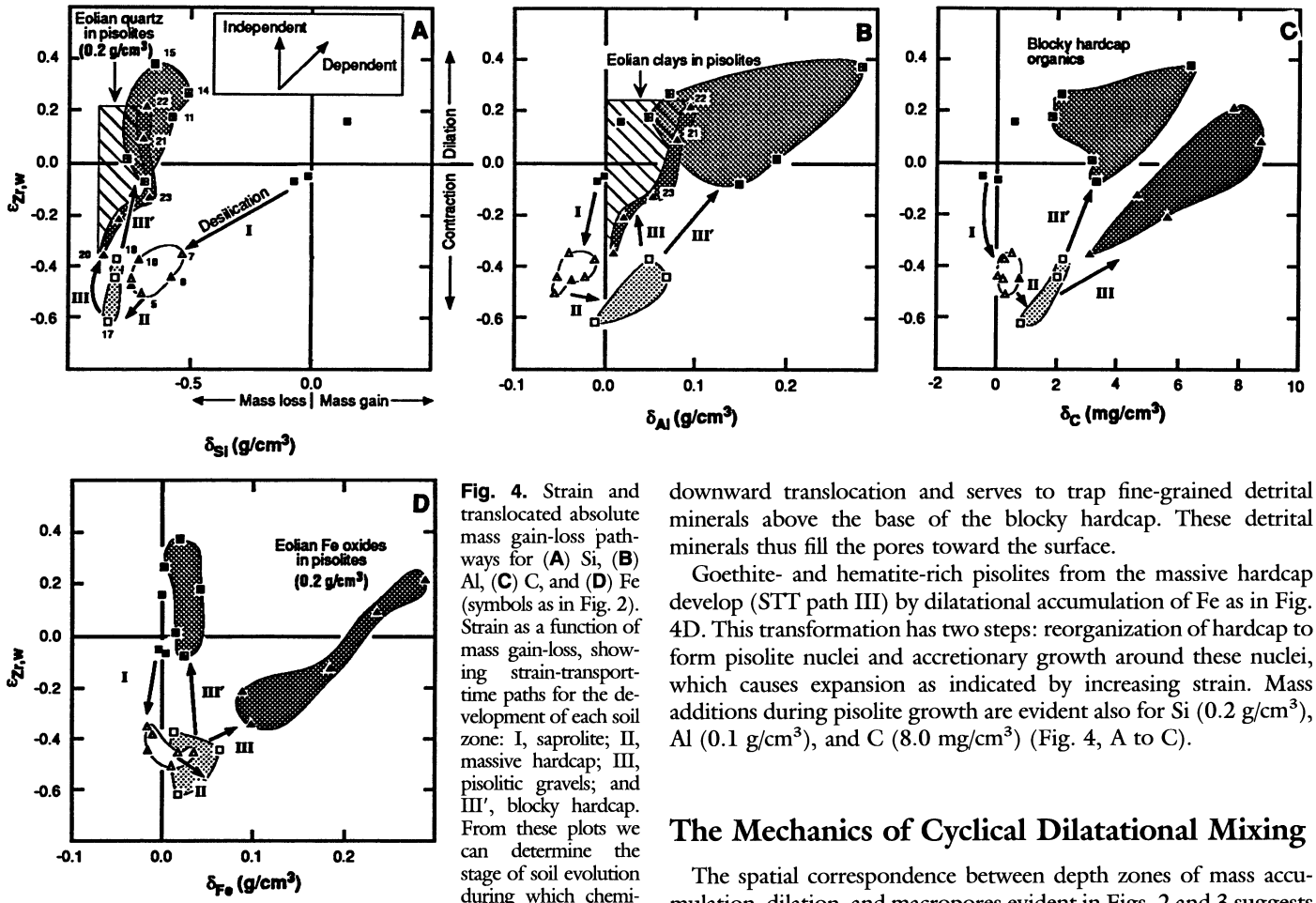

Fig. 4. Strain and translocated absolute mass gain-loss pathways for (**A**) Si, (**B**) Al, (**C**) C, and (**D**) Fe (symbols as in Fig. 2). Strain as a function of mass gain-loss, showing strain-transport-time paths for the development of each soil zone: I, saprolite; II, massive hardcap; III, pisolitic gravels; and III′, blocky hardcap. From these plots we can determine the stage of soil evolution during which chemical species contributed to deformation. Vertical slopes indicate that an element did not affect strain. The diagram is subdivided into four quadrants on the basis of the direction of deformation and mass gain or loss as indicated, with the point (0,0) being the origin protolith: upper left, expansion and mass loss; upper right, expansion and mass accumulation; lower left, contraction and mass loss; and lower right, contraction and mass accumulation.

losses of four major elements (Si, Al, C, and Fe) essentially control the state of strain from parent material to protosoil, to hardcap, and ultimately to pisolitic gravel.

Bedrock is first transformed to protosoil, which becomes more clay-rich toward the surface (pathway I in Fig. 4), a trend indicating a collapse of 50% that is induced by desilication (loss of 0.6 g/cm^3 of Si) during dissolution of feldspars (while quartz is retained). Collapse is accompanied by a minor loss of Al and no change in the mass of Fe. These stage I processes are equivalent to those responsible for the soil evolution in the beach sand discussed above.

The zone immediately above the protosoil, the blocky hardcap, is anomalous in terms of strain because it is dilated. It is an anomaly in the generalization that monotonic soil maturity increases upward. We infer that the transformation after parent material to protosoil is probably protosoil to massive hardcap (STT path II), a process involving only minor Si loss and no change in the state of strain (Fig. 2M), although Al, C, and Fe accumulate in minor amounts. We propose that the blocky hardcap, out of vertical maturation sequence, develops by modification of massive hardcap (STT path III′) by accumulation of Si, Al, and C compounds and no change in the amount of Fe. These changes occur by infilling of open voids, a process resulting in the microsedimentary features in Fig. 3F. A dramatic decrease in pore size in the protosoil restricts farther downward translocation and serves to trap fine-grained detrital minerals above the base of the blocky hardcap. These detrital minerals thus fill the pores toward the surface.

Goethite- and hematite-rich pisolites from the massive hardcap develop (STT path III) by dilatational accumulation of Fe as in Fig. 4D. This transformation has two steps: reorganization of hardcap to form pisolite nuclei and accretionary growth around these nuclei, which causes expansion as indicated by increasing strain. Mass additions during pisolite growth are evident also for Si (0.2 g/cm^3), Al (0.1 g/cm^3), and C (8.0 mg/cm^3) (Fig. 4, A to C).

The Mechanics of Cyclical Dilatational Mixing

The spatial correspondence between depth zones of mass accumulation, dilation, and macropores evident in Figs. 2 and 3 suggests that the mass transport processes controlling soil development are linked with deformation. The collective effect of many cycles of root growth and decay is progressive dilation when foreign particles added at the soil surface fill the pores created by roots, not only once but repeatedly, so that an excess volume of solids inflates the soil. During soil evolution, inflation develops in proportion to the subsurface space problem caused by continued translocation of mobile detritus or of precursors of chemical precipitates into voids in the subsurface. Relaxation or restoration of the system to an unstrained state is precluded because of the continued detrital influx. This dilatational effect may be enhanced by burrowing organisms, especially as mineral particles are excavated and transported above ground, contributing to further soil disaggregation (*40, 41*). This process results in a thorough mixing that attends inflation.

An understanding of dilatational mixing is central to evaluating deformational mass transport during soil evolution, but proof of its viability hinges on a demonstration (i) that the parent material is continuous, (ii) that the strain analysis is valid, shown by a demonstration of the chemical immobility of Zr in the strain index mineral used, zircon, (iii) that much of the detrital heavy-mineral fraction has a foreign source, and (iv) that the inferred mechanism is possible mechanically in light of known root-growth stresses.

The first three conditions involve use of the mineral zircon as a tracer. This mineral is useful because most of the Zr in the soil resides in this mineral, it is a common detrital mineral, and its age and surficial history can be determined with a combination of radiogenic isotope geochemistry and scanning electron microscope (SEM) analysis. Ion microprobe work has been done with the SHRIMP (sensitive high mass resolution ion microprobe) (*42*) (Fig. 5).

Three distinct types of zircon were evident in the cratonal soil: (i)

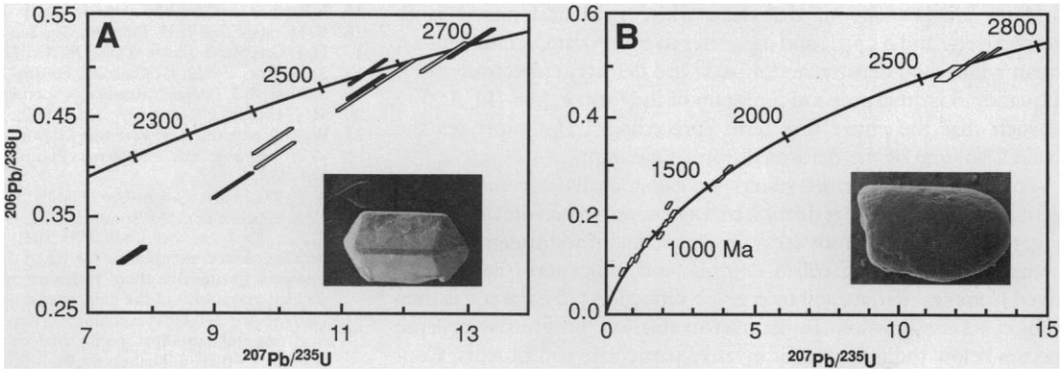

Fig. 5. Ion microprobe data on (**A**) zoned euhedral zircons from the Jarrahdale protolith gneiss (solid symbols; samples 1129-1 and 1129-4) and bauxite profile (open symbols; sample 1129-23), revealing continuity of Archean bedrock parent material, and on (**B**) clear, rounded foreign zircons, showing a wide provenance age spectrum down to 90 Ma. Insets: SEM images of (A) euhedral (170 μm) and (B) rounded (200 μm) zircon populations from Jarrahdale.

euhedral zircons occurring in the granitic parent bedrock, (ii) euhedral and color-zoned zircons occurring throughout the bauxite profile that appeared to be identical to the zircons in the granite, and (iii) colorless rounded zircons, found only from the surface down to a depth of 2 m within the pisolitic gravels and upper part of the blocky hardcap. The similarity of $^{206}Pb/^{238}U$, $^{207}Pb/^{235}U$, and $^{207}Pb/^{206}Pb$ ages as well as recent Pb loss patterns of both types of euhedral zircons in the gneiss and overlying bauxite demonstrate that the bauxite developed by weathering of the gneiss. In contrast, the broad age spectrum from 2600 to 90 Ma (million years ago) of rounded zircons (Fig. 5B) shows that they were derived from rocks of a foreign character. Analysis with the SEM shows that pristine euhedral zircon occurs throughout the profile and indicates that zircon is insoluble in the pore solutions. These data support the use of Zr in strain determination after the Zr profile is corrected for the younger rounded zircon introduced in the upper 2 m (*43, 44*).

We tested the feasibility of the proposed dilatational mixing mechanism by experimental simulation under dry conditions of root growth cycles and decay (Fig. 6A). We used fine-grained white sand positioned above a black-colored composite granular mixture consisting of hollow plastic spheres 1 cm in diameter and interstitial black sand; the mixture had a bulk density near that of soil. The dilatational mixing test cell contained a single vertical tube, a pseudoroot made of surgical rubber that was inflated with nitrogen gas at known pressure and deflated in cycles to simulate root growth; expansion or decay was separated by periods of translocation of surficial granular material. We found that a stress of approximately 11 bar was adequate to deform the sandy matrix. Natural root-growth pressures can approach 15 bar (*45*). At the start of the experiment, the interface between white sand and black porous substrate was sharp and horizontal (Fig. 6A). Mixing commenced with downward translocation of white sand through the black sand matrix during several cycles of expansion and contraction. The contraction phase of the tube cycle decompressed the surrounding matrix and allowed white sand particles to penetrate deeper into the black material as a propagating wedge of mixed sand.

As the number of cycles increased, a conical mixing front proceeded to greater depths (labeled 1 in Fig. 6B), defining the downward limit of translocation (*46*). The original interface between white and black sand began to ascend, indicative of cyclical dilatational mixing. After only 200 cycles, more than 3 cm of upward dilation indicates that the two-dimensional horizontal compressive stresses were readily converted into true three-dimensional vertical displacements, even in this simplified case with no water available to assist translocation.

Both dilation and mixing depth increased in proportion to the number of inflation-deflation cycles (Fig. 6C); the cycles were controlled at a rate of about 3 cycles per minute (a rate that was shown to be sufficiently slow to allow complete translocation). Dilation is directly proportional to the depth of mixing (Fig. 6D). These experimental results are consistent with an expression for strain ($\varepsilon_{i,w}$) that shows direct dependence on depth of mixing (Z_m) (Eq. 5)

$$\varepsilon_{i,w} = \left[\frac{\rho_s Z_m(\text{area})\ 100 + \rho_{g,p}(1 - n_p)C_{i,p}V_p}{\rho_{g,w}(1 - n_w)C_{i,w}}\right]\frac{1}{V_p} - 1 \qquad (5)$$

where area is horizontal cross-sectional area of a control volume, n_p

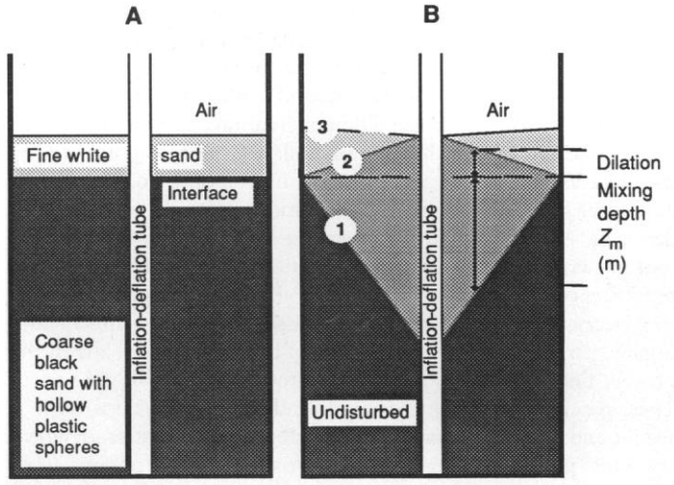

Fig. 6. Soil mechanics test cell used to simulate cyclical dilatational mixing. (**A**) The cell contained a surgical rubber tube embedded in a sandy matrix that was viewed through the front plastic panel of the mixing cell. (**B**) Essential features after dilation. Curve 1 is the depth of mixing at a certain number of cycles, curve 2 is the dilated surface, and curve 3 is the top of the overlying fine sand body. Results of cyclical dilatational mixing by translocation: (**C**) expansion (○) and depth of translocational mixing (●) as a function of number of cycles and (**D**) relation of expansion with mixing depth. From Eq. 5, strain should be directly proportional to translocational mixing depth, density of the translocating mineral grain (ρ_s), and average grain density of the parent material ($\rho_{g,p}$) and vary inversely with average grain density of the mixed material ($\rho_{g,w}$), its porosity (n_w), and the concentration of an immobile element ($C_{i,w}$).

and n_w are porosity of the clean white sand and mixed sand, respectively, and ρ_s, $\rho_{g,p}$, and $\rho_{g,w}$ refer to translocated grain density, clean white sand density, and mixed sand density, respectively (*47*). Equation 5 is an expression for strain of the form $\varepsilon_{i,w} = (V_w/V_p) - 1$ such that the entire first term (preceding $1/V_p$) expresses the overall volume of the deformed porous medium.

From these experimental results and earlier analytical results on soil profiles, we propose that dilation of soils occurs when animal burrowing, root growth, and root decay are coupled with additions of organic compounds, inorganic eolian detritus, and indigenous material derived from near surface soil by regolith reduction (*10*); the soil is then subject to compression. In contrast to dilation, progressive collapse occurs below the influence of invasive particulate constituents. Consequently, collapse dominates the lower portion of soils below the depth of root penetration and dilatational mixing.

Consequences of Deformational Mass Transport

Physiochemical calculations of bulk strain show that natural deformation of soil is widespread and is a phenomenon that must be considered a critical dimension of soil properties as well as an essential feature of profile differentiation. In addition to mixing soils, deformation is related to mass transport of material moving in suspension and solution in the presence of subsurface stresses, particularly those induced by near surface root growth and load compaction at depth.

As shown above, soils are differentiated into distinct layers with variable strain (either dilation or collapse) that is governed by translocational mass gains or losses in response to gradational biological activity and mineral dissolution under shallow overburden load. Near the surface, consecutive cycles of translocation and root growth produce incremental inflation as continued mass influx precludes complete relaxation of the soil. Increased porosity due to root decay, burrowing, and mineral dissolution allows mineral and organic particles to move to the base of the dilated layer, and in the process, finer grains, which translocate to a greater depth, are sorted. These processes lead to translocation-induced soil horizons, such as argillic and spodic horizons. Farther below, in the substratum where few roots penetrate, microporous protosoil forms by organic acid–mediated hydrolysis of soluble rock minerals. Exploitation of microstructural imperfections in minerals that survive chemical attack releases all but the least soluble elements with time. Soil growth occurs by intense biomechanical invasion through the activity of roots and burrowing organisms and through inflation and activation of this decomposed and softened precursor layer of soil.

REFERENCES AND NOTES

1. G. Sposito, *The Chemistry of Soils* (Oxford Univ. Press, New York, 1989), p. 3.
2. R. W. Arnold, I. Szabolcs, V. O. Targulian, Eds., *Global Soil Change, the Report of an IIASA-ISSS-UNEP Task Force on the Role of Soils in Global Change* (International Institute of Applied System Analysis, Laxenburg, Austria, 1990).
3. B. G. Rozanov, *Soil Cover of the Earth* (Publishing House of the Moscow University, Moscow, 1977).
4. H. Jenny, *Factors of Soil Formation* (McGraw-Hill, New York, 1941).
5. _____, *The Soil Resource, Origin and Behavior* (Springer-Verlag, New York, 1980), pp. 151–159.
6. W. H. Emmons, *The Principles of Economic Geology* (McGraw-Hill, New York, 1918).
7. G. H Brimhall, C. N. Alpers, A. B. Cunningham, *Econ. Geol.* **80**, 1227 (1985).
8. G. H Brimhall and W. E. Dietrich, *Geochim. Cosmochim. Acta* **51**, 567 (1987).
9. G. H Brimhall *et al.*, *Nature* **333**, 819 (1988).
10. G. H Brimhall *et al.*, *Geoderma* **51**, 51 (1991).
11. O. A. Chadwick, G. H Brimhall, D. M. Hendricks, *Geomorphology* **3**, 369 (1990).
12. G. Millot and M. Bonifas, *Serv. Carte Geol. Alsace Lorraine Bull.* **8**, 3 (1955).
13. G. Millot, *Geology of Clays* (Springer-Verlag, New York, 1970), pp. 118–131.
14. There are instances in which physical strain markers such as intersecting veins confirm isovolumetric weathering, but, in general, such convenient physical strain markers are absent.
15. I. Barshad, in *Chemistry of the Soil*, F. E. Bear, Ed. (Reinhold, New York, 1964).
16. B. D. Soane and J. D. Pidgeon, *Soil Sci.* **119**, 376 (1975).
17. D. J. Greenland, *Philos. Trans. R. Soc. London Ser. B* **281**, 193 (1977).
18. S. M. Ross and D. C. Malcolm, *Forestry* **55**, 155 (1982).
19. S. Ross, *Soil Processes* (Routledge, London, 1989).
20. M. J. Knight, *Geoderma* **23**, 245 (1980).
21. W. D. Nettleton, F. F. Peterson, G. Borst, in *Soil Micromorphology*, P. Bullock and C. P. Murphy, Eds. (Academic Publishers, Berkhamsted, England, 1983), pp. 441–458.
22. A. L. Washburn, *Geocryology* (Halsted Press, New York, 1980), p. 97.
23. C. A. Alpers and G. H Brimhall, *Econ. Geol.* **84**, 229 (1989).
24. _____, *Geol. Soc. Am. Bull.* **100**, 1640 (1988).
25. Because of tectonic uplift in the lee of the Mendocino triple junction, flights of emergent Quaternary shore platforms are notched and preserved in the easily abraded graywackes of the Franciscan coastal terrane (*26*). Ages of the six terraces span the past 240,000 years (*26*) and were obtained from two methods, radiometric dating and altitudinal spacing analysis. The youngest terrace is assigned an age of 3.9 ka (+0.1/−3.9 ka) on the basis of shells found in original growth position. The remaining terraces are assigned inferred ages of 29, 40, 118, 124, 214, and 240 ka on the basis of correlation with dated worldwide glacio-eustatic sea-level highstands (*26, 27*). Error estimates are +5/−15 ka for the 29- to 124-ka terraces and +15/−20 ka for the 214- and 240-ka terraces (*26, 27*). The northern California coastal region has a cool, temperate, Mediterranean climate; mean annual temperature is about 13°C; mean annual precipitation is about 1 m (*28*). Climatic variations between glacial and interglacial periods are minimized by maritime influences on temperature. CLIMAP (Climate: Long-Range Investigation, Mapping, and Prediction) data indicate that full-glacial (18 ka) sea-surface summer (August) temperatures (13°C) were similar to modern sea-surface summer temperatures (~13°C; <1°C difference); however, winter temperature gradients were intensified, and full-glacial winter (February) sea-surface temperatures (7°C) were 4°C cooler than the modern winter temperature (11°C) (*28*). Modern mean summer (August) and winter (February) temperatures onshore are 13° and 8.5°C, respectively. Full-glacial precipitation may have been greater than at present because of steepened north-south temperature gradients. Present vegetation on the terraces is prairie bunch grasses. Full-glacial vegetation may have been coniferous trees (*29*), but the soil profiles suggest that there has been little vegetation change.
26. D. J. Merritts, O. A. Chadwick, D. M. Hendricks, *Geoderma* **51**, 241 (1991).
27. D. J. Merritts and W. B. Bull, *Geology* **17**, 1020 (1989).
28. *Geological Society of America Map and Chart Series*, no. 36 (1981).
29. D. L. Johnson, *Quat. Res. (N.Y.)* **8**, 154 (1977).
30. S. T. Trudgill, *Soil and Vegetation System* (Clarendon, Oxford, 1977).
31. A. Kabata-Pendia and H. Pendias, *Trace Elements in Soils and Plants* (CRC Press, Boca Raton, FL, 1984).
32. J. Richter, *The Soil as a Reactor, Modeling Processes in the Soil* (Catena-Verlag, Cremlingen, Germany, 1987).
33. P. L. C. Grubb, *Econ. Geol.* 66, 1005 (1971).
34. G. H Brimhall and M. L. Rivers, U.S. Patent 4,503,555 (1985).
35. G. H Brimhall and L. J. Vigus, U.S. Patent 4,521,308 (1985).
36. G. H Brimhall and C. J. Lewis, "Bauxite and laterite soil ores," in *Encyclopedia of Earth System Science* (Academic Press, San Diego, CA, in press).
37. This TCO behavior is invisible in conventional chemical profiles that do not incorporate strain and physical properties into a true mass gain and loss analysis. Here it is due to intense collapse at the base of the bauxite profile (Fig. 2M).
38. C. C. Nikiforoff, *Soil Sci.* 67, 219 (1949).
39. C. R. M. Butt, in *Geochemical Exploration in Deeply Weathered Terrains*, R. E. Smith, Ed. (Commonwealth Scientific and Industrial Research Organisation, Wembley, Australia, 1983), pp. 41–50.
40. The role of root growth, animal burrows, and tree throw heave in the generation of low-density porous soil material on hillslopes undergoing active erosion has been interpreted as mechanical disruption.
41. W. E. Dietrich and T. Dunne, *Z. Geomorphol. Suppl.* **29**, 191 (1978).
42. W. Compston, I. Williams, C. J. Meyer, *J. Geophys. Res.* **89** (suppl. B), 525 (1984).
43. Zircon insolubility should be established on a case-by-case basis because SEM studies on podzols (*44*) suggest that zircon can be pedogenically modified under extreme circumstances.
44. M. S. Tejan-Kelly, R. W. Fitzpatrick, D. J. Chittleborough, *Catena* **18**, 11 (1991).
45. R. S. Russell, *Plant Root Systems: Their Function and Interaction With the Soil* (McGraw-Hill, London, 1977).
46. The latex surgical rubber tube (0.95 cm outside diameter) from McMaster-Carr Company (Los Angeles, CA) was sheathed in a flexible braided polyester sleeve to minimize damage upon occasional bursting. The dimensions of the sand column inside the experimental cell were 72 cm high by 16.3 by 10 cm.
47. A particularly good example of this mixing effect is the particulate gold concentrated in the zone of lateritic weathering above mineralized Precambrian volcanosedimentary greenstone protoliths in the Yilgarn block of Western Australia and in the West African craton in Mali (*10*). It appears that because of small particle size and unusually high grain density, gold particles contained in the parent material are effectively enriched mechanically during regolith reduction as captive constituents in the laterite column.

48. We thank W. Gardner and H. Jenny for constructive comments; T. Teague for exquisite soil thin sections; J. Hampel for analytical measurements; B. Hallet for useful comparisons with solifluction; E. Pendall, D. Merritts, T. Dunklin, and J. Crittenden for assistance in the field; and K. Gross and L. Feldman for useful discussion of root systems. R. Anderson and M. Pavich provided insightful and careful reviews of the manuscript. Support from NSF grants EAR 8416790, 8804136, and 9018747 and from NASA Land Processes Division is gratefully acknowledged, as is funding from BHP-Utah International Metals.